12-2011

A Model For Rapid Charging Events on International Space Station

Debrup Hui
Utah State University

A MODEL FOR RAPID CHARGING EVENTS ON INTERNATIONAL SPACE STATION

by

Debrup Hui

A report submitted in partial fulfillment
of the requirements for the degree

of

MASTER OF SCIENCE

in

Electrical Engineering

Approved:

Dr. Charles M. Swenson Major Professor	Dr. Edmund Spencer Committee Member

Dr. Chris Winstead
Committee Member

UTAH STATE UNIVERSITY
Logan, Utah

2011

Abstract

A Model For Rapid Charging Events on International Space Station

by

Debrup Hui, Master of Science

Utah State University, 2011

Major Professor: Dr. Charles M. Swenson
Department: Electrical and Computer Engineering

Surface charging by plasma can be a serious issue for any spacecraft. Though significant charging is not observed in all spacecrafts at all times, it only requires a single episode of extreme charging to result in serious damage. The International Space Station (ISS) is an interesting platform to study these charging effects because of its size and relatively high voltage systems. Of the many kinds of charging observed on ISS, the rapid charging events during solar eclipse exit in a low-density ionosphere is not yet understood. This report is an investigation to understand this phenomenon. This report proposes a simple linear model of this nonlinear charging that takes into account the capacitive and resistive natures of conducting and oxidized surfaces is sufficient to describe the phenomenon.

(53 pages)

Public Abstract

A Model For Rapid Charging Events on International Space Station

by

Debrup Hui, Master of Science

Utah State University, 2011

Major Professor: Dr. Charles M. Swenson
Department: Electrical and Computer Engineering

Surface charging by plasma can be a serious issue for any spacecraft. Though significant charging is not observed in all spacecrafts at all times, it only requires a single episode of extreme charging to result in serious damage. The International Space Station (ISS) is an interesting platform to study these charging effects because of its size and relatively high voltage systems. Of the many kinds of charging observed on ISS, the rapid charging events during solar eclipse exit in a low-density ionosphere is not yet understood. This report is an investigation to understand this phenomenon. This report proposes a simple linear model of this nonlinear charging that takes into account the capacitive and resistive natures of conducting and oxidized surfaces is sufficient to describe the phenomenon.

To my mother who first taught me to look at the stars . . .

Acknowledgments

At this stage of my career, when I sit down and try to recollect my journey as a graduate student at Utah State, I strongly feel the urge to thank all my professors and colleagues who have helped me throughout this journey. Without their help and support, this report could not have taken the current shape.

First and foremost, I extend my heartfelt gratitude to my thesis advisor, Prof. Charles Swenson, who not only defined the dimensions of the project but also was always there to help me overcome every stumbling block I faced during this research, whose involvement held my interest and enthusiasm in this project throughout the last two years. I am indebted to him for his invaluable guidance. Thank you, Chuck, for all your help.

I also thank Prof. Edmund Spencer and Prof Chris Winstead, who not only took interest in my research and served on my thesis committee but also trained me on different research-related subjects throughout my master's program over the last two years.

I extend my heartfelt thanks to Leonard Kramer and group, Boeing Corporation, for discussing different research related things with our group from time-to-time. I also thank my friends whose moral support and inspiration kept me going at times when I felt low. Thanks go to Ashish, Prajwal, Rajendra, Steve, Nimish, and Amrita!

I take this opportunity to thank Chad Fish from SDL for his support and inspirations from time-to-time. My acknowledgement would be incomplete without thanking Trent Johnson for his constant technical support and Mary Lee Anderson for her administrative support all along.

Last, but not least, I thank my family back in India for their constant understanding and support without whom this journey would not have been possible.

Debrup Hui

Contents

List of Tables

List of Figures

Notations

R	Resistance
C	Capacitance
ϵ_0	Permittivity of free space
ϵ_r	Relative permittivity
k	Boltzmann constant
T	Temperature in ° Kelvin
A	Area
n	Plasma density
e	Electronic charge
V_{ISS}	ISS orbital velocity
B	Earth's magnetic field strength
d	Thickness of dielectric layer
λ	Debye's length
J	Current density
J_{ph0}	Photoelectron current density
ISS	International Space Station

Acronyms

ISS	International Space Station
FPMU	Floating Potential Measurement Unit
FPP	Floating Potential Probe
NASA	National Aeronautics and Space Administration
USU	Utah State University
CS	Conducting Surface
INS	Insulated Surface
SA	Solar Array
NCE	Normal Charging Event
RCE	Rapid Charging Event
PVA	Photovoltaic Array

Chapter 1

Introduction

Every day we are taking small steps towards a world which depends ever more on satellites than yesterday. After a few decades of space flight, "Space" still remains a big challenge to human beings. With a vision to make space our permanent home, humans strive to master the science and technology to overcome the dangers it can pose to our missions. Up in space, spacecraft, whether manned or unmanned, faces a very different environment than on earth, which might be the cause of failures for its systems. A critical threat is the phenomenon of *spacecraft surface charging*. Spacecrafts get charged in the space environment due to the surrounding plasma and if this charging reaches a critical limit can damage or destroy the spacecraft systems. The International Space Station (ISS), (Fig. 1.1), because of its size and accessibility, is an important platform to observe and understand events that any spacecraft can experience. The space environment through which satellites orbit is full of charged particles, electrons and ions, which constitute the *space plasma*. The electrons move much faster than ions due to their low mass, and therefore collide with the surface of the satellite more frequently than ions thus depositing a net negative charge. A body immersed in such plasma develops a potential *floating potential* with respect to the surrounding plasma that repels some of the electrons until balance with the ions colliding with the surface is achieved. The ISS is the largest manmade body orbiting the earth in space and with its huge capacitance to surrounding plasma it stores large amount of charge on its surface. The stored charge results in a floating potential of few tens of volts relative to the surrounding plasma (see [1,2]) superimposed on the charging already caused by the motion of ISS in earth's magnetic field called $V \times B$ charging (more details are given in Section 1.1.2). The amount of stored charge could prove fatal to the safely of the crew and also to the accuracy of the onboard instrument measurements. The negatively

grounded high voltage Photovoltaic Arrays (PVA), its size, human presence, oxide coating, and onboard experiments demand for a close monitoring and control of the charging effect for the ISS [1]. Two units of Plasma Contractors (PCU) has been installed onboard ISS to get rid of excess charges back into the space, thereby lowering the floating potential with respect to the surrounding plasma [3].

An instrument called the Floating Point Measurement Unit (FPMU) has been installed on ISS since August 2006 to monitor the level of spacecraft charging. Although the charging of the ISS is generally understood, there are unexplained charging events observed by the FPMU. One of the charging features in FPMU data is called a Rapid Charging Event (RCE). A RCE is a charging event when the spacecraft gets charged within seconds, especially in low-density regions during eclipse exit or when the solar panels become energized in sunlight. A more detailed discussion is given in the following section. This report presents a nonlinear model of this charging process for ISS which can explain occurrence of such charging-discharging events. The report discusses in detail a linearized version of this model including its scope and limitations and the need for an advanced solution of the nonlinear model. In the following sections we present a discussion of the ISS structure and of the different kinds of charging phenomena observed on the ISS by the FPMU. This would be followed by a section describing the theory and mathematics of collection currents by any surface surrounded by plasma.

1.1 ISS Charging and RCEs

1.1.1 The ISS Structure

The ISS is an international research facility built in the low earth orbit by NASA. The on orbit construction started in 1998 and since then various modules have been added to it. The evolution of ISS can be viewed from different angles, but for the purpose of studying the charging of the station, which is a surface phenomenon, the increase of its surface area consisting of either glass-covered solar array, bare metal, or oxide coated are important. For example, of the four pairs of solar arrays presently installed on ISS, the

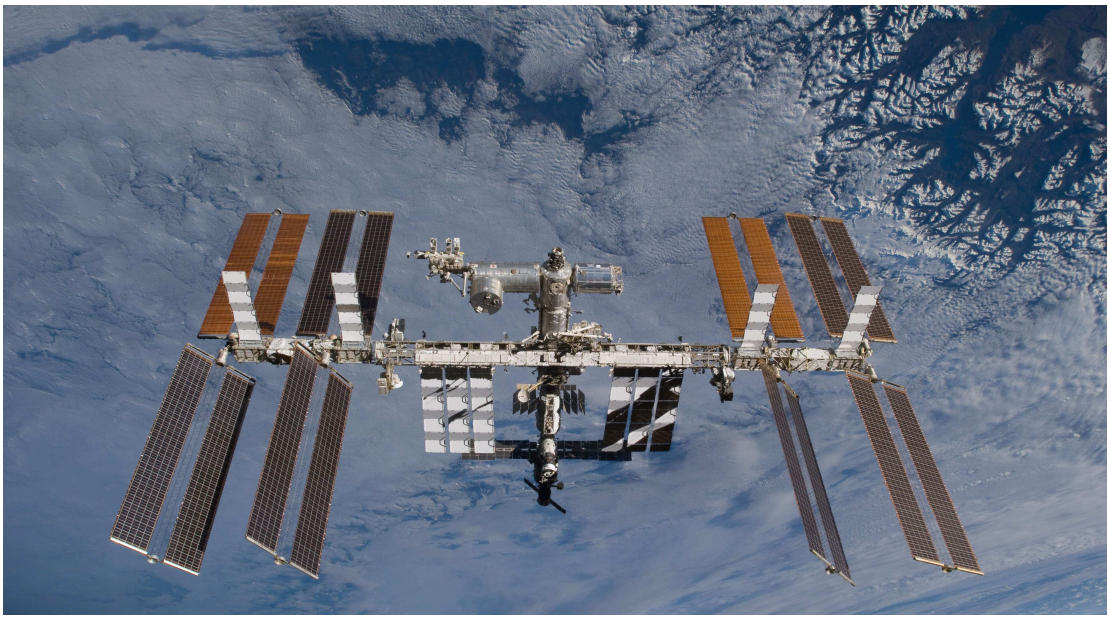

Fig. 1.1: International Space Station.

first pair was installed in 2000, second in 2006, third pair in 2007, and the fourth pair in 2009. So the glass-covered area, which is an important source of charging as we will discuss in coming chapters, increased considerably over time. Similar things happened with conducting surfaces and anodized/oxidized surfaces. So to understand the charging problem on ISS, it is very important to keep track of these changing surface areas. Figure 1.2 gives an idea of the slow evolution of ISS structure.

1.1.2 ISS Charging

The FMPU designed and built by Utah State University (USU) has been placed on the ISS to monitor the floating potential of the spacecraft and the conditions of the local plasma Fig. 1.3. The FPMU is a package of four plasma instruments:

- the Floating Potential Probe (FPP),
- the Plasma Impedance Probe (PIP),
- the Wide-sweep Langmuir Probe (WLP), and
- the Narrow-sweep Langmuir Probe (NLP) with associated electronics.

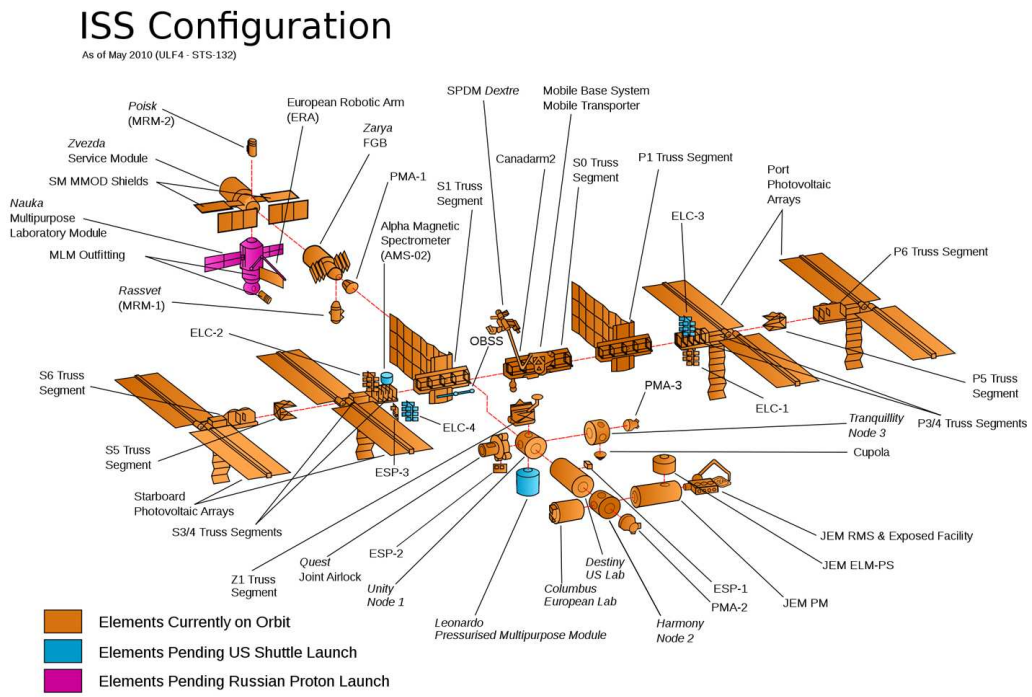

Fig. 1.2: ISS construction as of May 2010.

These probes also monitor the local plasma temperature, density, and electric fields. A more detail about the FPMU instruments and observations have been discussed in literature [4–7]. The data showing the charging phenomena below are based on floating potential data collected with the FPP [1].

Types of ISS Charging

The different types of charging observed on ISS as the station slowly grew up over the years are discussed in detail in Craven et al. 2009. Based on the FPP data collected between August 2006 and November 2008 in different campaign mode totaling 167 days, five different kinds of charging could be identified. A list of the days when these data were collected is given in Table 2 [1]. Important to mention, this was a period of solar minimum (Cycle 23) and the geomagnetic index Kp was rarely over 4. Also to be noted, the structure of ISS, which also influences the charging of the spacecraft, was changed during this period due to relocation and addition of PVAs and addition of new modules [1].

The different charging events which are the results of the interaction of the ISS structure with the surrounding magnetic field, plasma, operation of PVAs, geophysical conditions, and onboard experiments, can be categorized.

- **Magnetic Induction:** It is the induction produced because of the spacecraft's motion through the earth's magnetic field and is given by $V_{ISS} \times B \cdot L$, where V_{ISS} is the velocity of the ISS and B is the earth's magnetic field at that location, and L is the position vector of FPMU. This is a sinusoidal-like variation as reproduced in Fig. 1.4.

- **Equatorial:** Within the region of Appleton Anomaly in the equatorial sector with enhanced electron density and reduced temperature, the ISS experiences potential enhancement. This is due to enhanced electron collection by the PVAs [8]. This occurs mostly during or near local noon and superimpose up to few volts of floating potential over magnetic induction described earlier [1].

- **High Latitude:** While crossing the magnetic high latitudes, the ISS experiences some charging events as described in Fig. 3 [1]. These are thought to be from incoming high energy particles especially during geomagnetic or solar storms.

- **Unusual Events:** During addition (called docking) of extra modules to the main station or during active experiments which generates plasma in the local environment the floating potential has been found to increase [1, 9].

- **Eclipse Exit:** Charging has been recorded when the ISS enters sunlight from eclipse [10,11]. The transient negative potential increases rapidly as the ISS leaves the earth's shadow and enters sunlight at morning terminator, especially, when the PCUs are not operating. Depending on the rate of transition such events are further divided into Normal Charging Events (NCEs) which are characterized by a charging rise time of 10s of seconds and the discharge (fall) cycle of several minutes depending on the PVAs condition and local plasma conditions. An example of NCE is shown in Fig 1.5 (a). The other type of charging, which is the central topic discussed in this paper is called Rapid charging Events (RCEs) characterized by a rise time of < 10 secs (usually 2-3

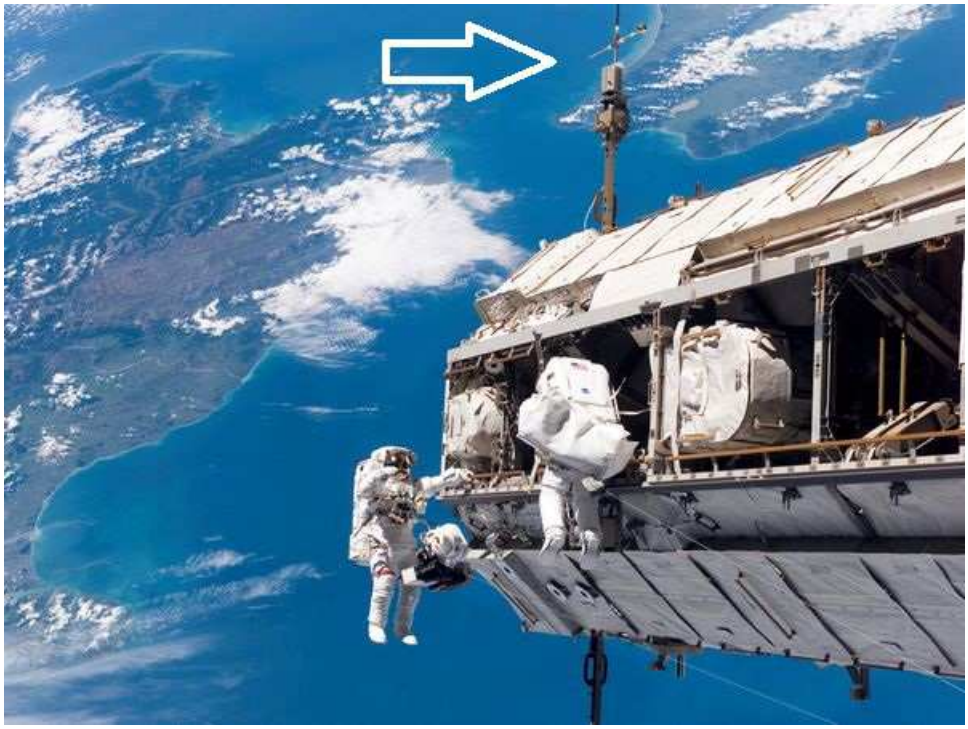

Fig. 1.3: The white arrow shows the FPMU instrument onboard ISS.

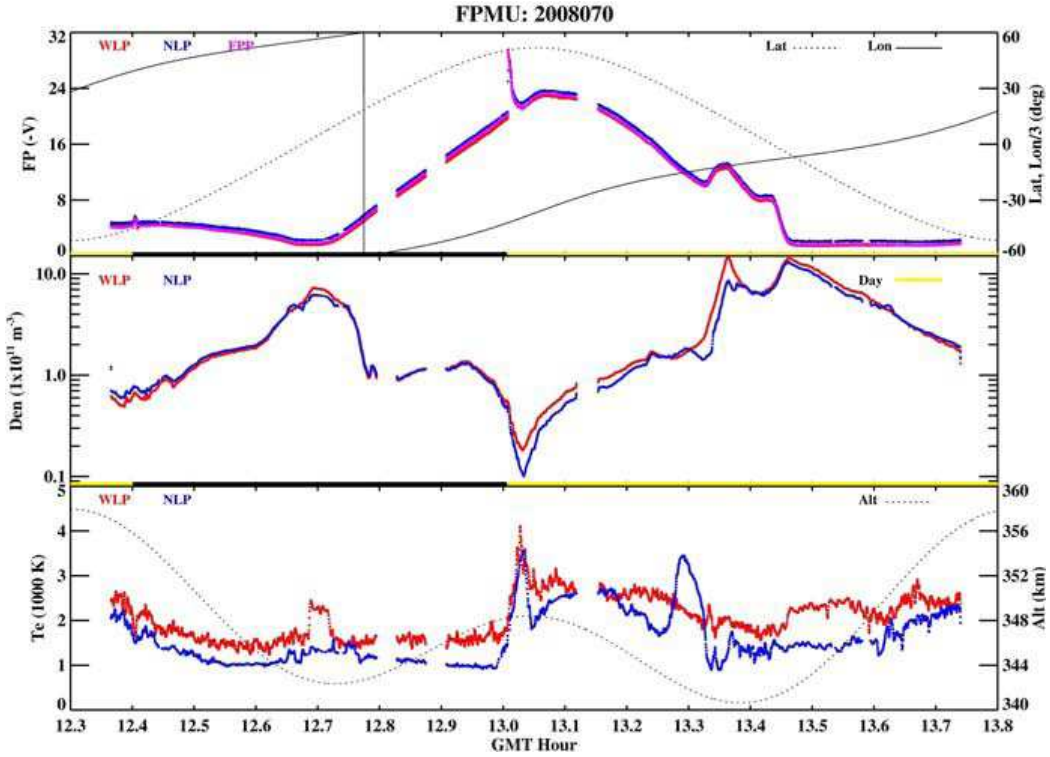

Fig. 1.4: Magnetic induction charging and eclipse exit charging.

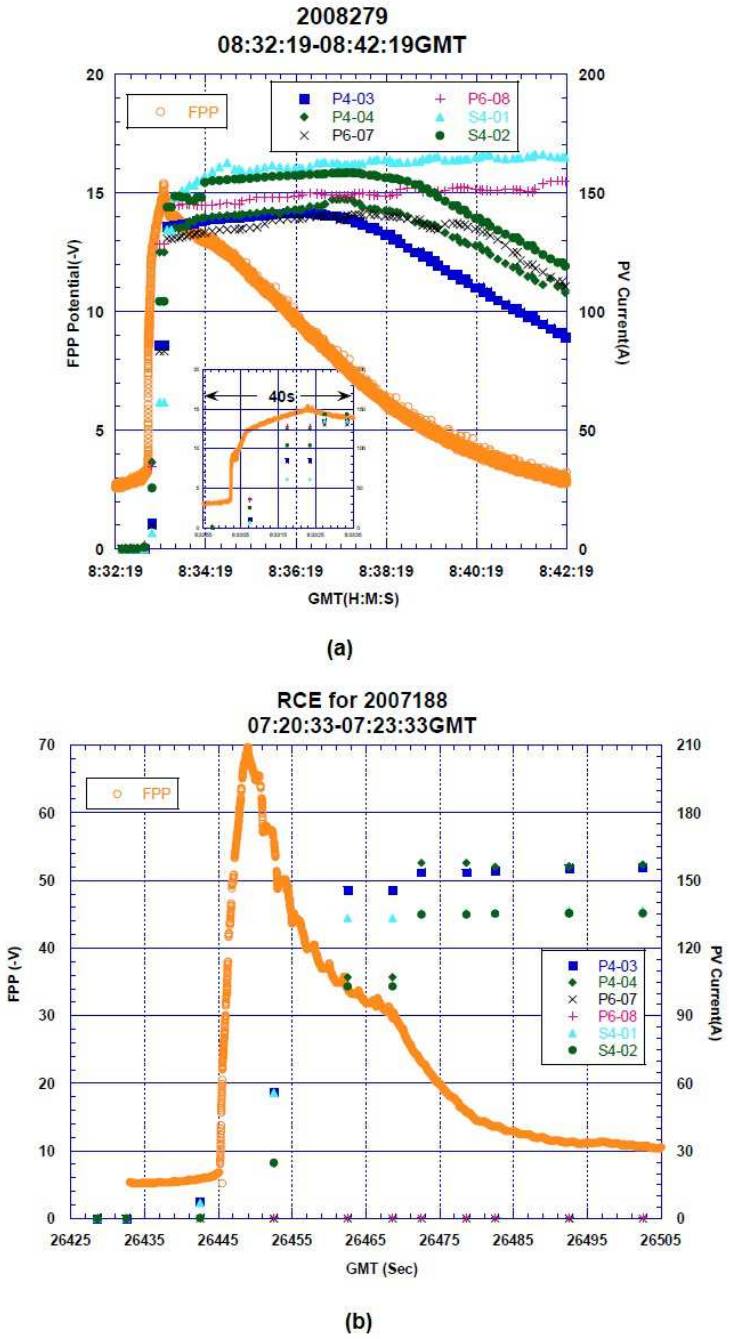

Fig. 1.5: (a) Top and (b) bottom panel: Example of NCE and RCE. The Y-axis on the left of each plot describes the floating potential, where as the Y-axis on the right denoted the currents at each PVAs onboard ISS.

seconds) and fall time of few 10s of seconds. Such RCEs are recorded on 44 days during the period mentioned before with multiple events on the same day. RCEs are mainly observed during the eclipse exit where the density is less than $< 3.5 \times 10^{10} m^{-3}$ [1]. Such densities occur in the depletion regions found at higher geographic latitudes ($|latitude| > 37°$) or at equatorial latitudes ($|latitude| < 17°$). Figure 1.5(b) shows an example of RCE of July 7, 2007, when the maximum amplitude REC is recorded till date. In both the figures, the PVA currents are shown in the right Y-axis. A more detailed description about this can be found [1].

1.2 Theory of Collection Currents

1.2.1 The Mathematical Background

The reason for RCEs is not well understood. To model such events we consider the collection of currents from a mesothermal plasma ($v_{ti} << v_d << v_t$) in which the drift velocity of plasma particles in between ion thermal and electron thermal velocity. The electrons are described by a stationary maxwellian distribution and the ions found in low earth orbit are assumed to be of drifting maxwellian distribution and nearly monoenergetic Fig. 1.6. The photoelectrons to be emitted from the surface of ISS are also assumed to be stationary maxwellian distribution [12]. Radiation in the space environment due to high energy electrons also produces currents to a surface either by direct collection or by ejecting multiple electron of the surface through processes such as backscatter and secondary emission. The floating potential of a surface is determined from the current balance equation [12, 13]

$$I_{net}(\phi_0) = I_e(\phi_0) - I_i(\phi_0) - I_{se}(\phi_0) - I_{si}(\phi_0) - I_b(\phi_0) - I_{ph}(\phi_0) = 0, \tag{1.1}$$

where ϕ_0 is the surface floating potential, I_{net} the total current, I_e the electron current, I_i the ion current, I_{se} the secondary electron current due to I_e, I_{si} the secondary electron current due to I_i, I_b the backscattered electron current due to I_e, I_{ph} the photoelectron

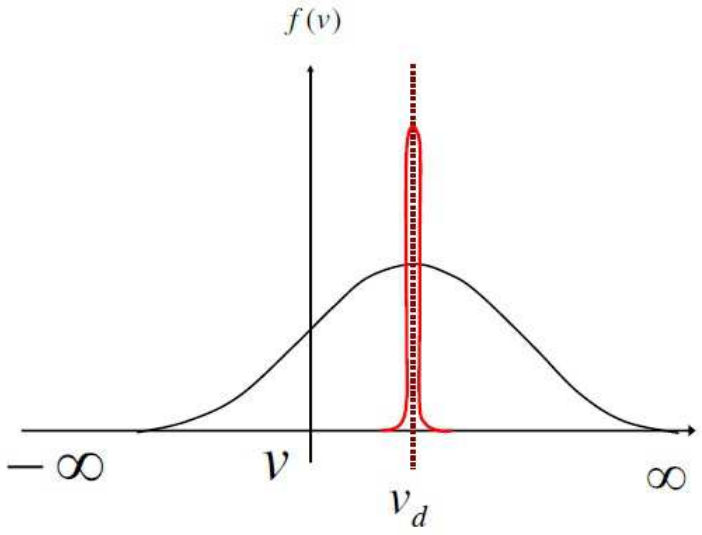

Fig. 1.6: Distribution functions for electrons (black) and ions (red).

current.

For the nonlinear model (of which the present linear model is a derivative), we neglect the secondary currents due to electrons and ions and the backscattered electron current. We only consider the ambient electron current, ambient ion current, and the photoelectron current.

1.2.2 Collection Currents

The current per unit area collected by an object immersed in plasma depends upon the potential of the object relative to the undisturbed plasma as well as density and temperature of the plasma. If this potential is zero then the collected current is called the saturation current. For a maxwellian distribution of the type

$$f_j(v) = n_j \left[\frac{m_j}{2\pi k T_j}\right]^{\frac{3}{2}} exp\left[-\frac{m_j(v_x^2+v_y^2+v_z^2)}{2kT_j}\right]. \tag{1.2}$$

The saturation current density, J_j, for the species collected for a plane surface is given by

$$J_{j0} = q_j \int_{-\infty}^{\infty}\int_{-\infty}^{\infty}\int_{-\infty}^{\infty} \vec{v}.\vec{n} f_j(v) dv_z dv_y dv_x = q_j n_j \sqrt{\frac{kT_j}{2\pi m_j}}. \tag{1.3}$$

And the current density for the species repelled by the plate when charged to surface potential (ϕ_0) is given by

$$J_j = J_{j0} exp\left[-\frac{q_j \phi_0}{kT_j}\right], \tag{1.4}$$

where q_j, n_j, m_j, T_j are charge, density, mass, and temperature for a species "j" and k is Boltzmann's constant. To get the total current collected, we must multiply these density functions by the collecting area. When the potential on the surface is attracting species, the current collected depends upon the shape and size of the object relative to the plasma sheath surrounding the object by Orbit Motion Limited (OML) theory. If the sheath is much larger than the object then the current collected is given by the following equations:

$$J_j = J_{j0}\left(1 + \frac{-q_j \phi_0}{kT_j}\right)^{\beta}, \tag{1.5}$$

where for a flat plate, $\beta = 0$; for a cylinder, $\beta = 1/2$; and for a sphere, $\beta = 1$. If the object is much larger than the plama sheath, then the collection tends towards the flat plate, $\beta = 0$, regime. The equation for a cylindrical object given the sheath and object size is given by OML theory as

$$J_j - J_{j0} = \left(\frac{s}{R_p} erf\left(\frac{-q_j \phi_0}{kT_j}\left(\frac{s^2}{R_p^2} - 1\right)^{-1}\right)^{\frac{1}{2}} + erfc\left(\frac{-q_j \phi_0}{kT_j}\left(1 - \frac{R_p^2}{s^2}\right)^{-1}\right)^{\frac{1}{2}}\right), \tag{1.6}$$

where R_p is the size of the object, and s is the dimenstion of the sheath, and erf and $erfc$ are the error function and complementary error function, respectively. For a spacecraft moving at an orbital velocity v_i, the thermal velocity of the electrons is still faster, but the thermal velocity of the ions is slower. This is known as a meso-thermal plasma. The ion current collected by a surface in such drifting maxwellian plasma under OML theory is complex. This collection current for ions under simplifying assumptions becomes [14]

$$J_j = n_i q_i v_i \pi^{-1}\left(1 + \frac{kT_j}{mv_i^2} + \frac{2e\phi_0}{mv_i^2}\right)^{\frac{1}{2}}. \tag{1.7}$$

For a spacecraft in the lower earth orbit, the dominant currents are due to the ions and electrons collected given by above equations. Other sources can be considered, such as photoelectrons or radiation induces currents though their magnitudes are small compared to these thermal currents. The current balance equation can be written as

$$0 = J_e + J_i + J_{Ph0}, \tag{1.8}$$

where J_{Ph0} represents the photocurrent. The potential that a spacecraft reaches at steady state is defined by this current balance equation as was mentioned in the beginning.With this mathematical background and few physical assumptions as made in the next section, our next step is to develop a equivalent electrical circuit model for ISS to simulate RCEs.

1.3 Our Model for RCEs and Report Overview

The charging of ISS has been studied over last few years by many. The FPMU data has helped understand the charging of ISS. Different charging phenomenon on ISS are reported in literature [7, 8, 11, 15]. Five different types of charging being observed on ISS includes RCEs [1]. The RCEs has been also been reported and studied by many [2, 16]. The only serious theory published till date for RCEs which further elucidates the charging of spacecrafts in LEO environment is by D. C. Ferguson and coworkers [16]. Predictions of future RCEs under different solar conditions were made using this model and are ready for onboard testing. The model points out that such charging takes place because of the nonequilibrium condition of the solar arrays with its surrounding. Our model, developed and described in this report, takes into account the whole ISS system as an electrical system and verifies contribution from different surfaces towards such events. It is the first such attempt to describe ISS as a very simple electric circuit to understand its charge exchange with surrounding plasma as far as RCEs are concerned. The model can also be used to make estimations and predictions for future RCEs not only on ISS but any big spacecraft in LEO environment. This is important to avoid sudden overcharging of the station and also to avoid dielectric breakdown of surface insulations. So to understand the reasons for

such events and to predict future events our model will come very simple and effective.

This report is divided into different chapters. In Chapter 1, we introduced the problem of RCEs and discussed the structure of the ISS, the instrument FPMU, and the different kinds of charging ISS experiences while orbiting in low earth orbit. The theory of collecting currents by any surface in space plasma environment is discussed. In the first section of Chapter 2, a linear electric circuit model of ISS is developed from the physical system to explain the charge exchange of ISS with its surroundings. This electric circuit model shows in the light of collection currents why and how RCEs can be observed onboard ISS. The second section in Chapter 2, an attempt is made to study analytically using mathematics of circuit analysis to understand the RCEs and the possible elements causing the same. The contribution and values of different important elements in the system are discussed. In Chapter 3, the simulation results of RCEs using the developed linear model is presented and discussed. Chapter 4 concludes the report with important lessons learned from this research. The need of a more advanced nonlinear model to address the problem of RCEs is also discussed.

Chapter 2

Developing a Model for RCEs

2.1 Electric Circuit Model

The RCEs happen because of dynamic changes in the accumulation of charges on the surface of ISS from the surrounding space plasma. The dynamic changes are caused by the energization of the ISS solar panels relative to the rest of the ISS structure. The RCE events can only be understood by understanding the system of exchange of charges between ISS components and the surrounding plasma. The first step towards understanding RCE requires the development of a practical electrical circuit model for ISS. To do this we breakdown the surface of the ISS into four components: a) Insulated/oxidized surface, b) Conducting metal surface exposed to plasma, c) The outside of the glass-covered solar array surface, and d) The inside conducting surface of the solar cells. The surface area of the Floating Potential Probe of the FPMU, which measures the floating potential of the ISS, is also included in the model for completeness in understating its data. The insulated and conducting surfaces are assumed for current collection purposes to be cylindrical, the solar array to be a plane surface, and the probe is assumed to be spherical in shape. These geometries are important in the application of collection current equations in the nonlinear model. In the linear model, we will not directly address these differences. Four of these surfaces (P1, P3, P4, P5) separately draw currents from the plasma which is a function of the potential difference between the plasma and the respective surface as illustrated in Fig. 2.1. The surface P2 is isolated from the plasma by the cover glass on the solar cells but is connected through a voltage source, the solar cells, to the rest of the ISS conductive structure. The probe is electrically separated from the main spacecraft body by a huge resistance ($> 10^{15}$ ohms - shown as R_{PR} in Fig. 2.2).

Two important things to note here are that each surface will develop a sheath around

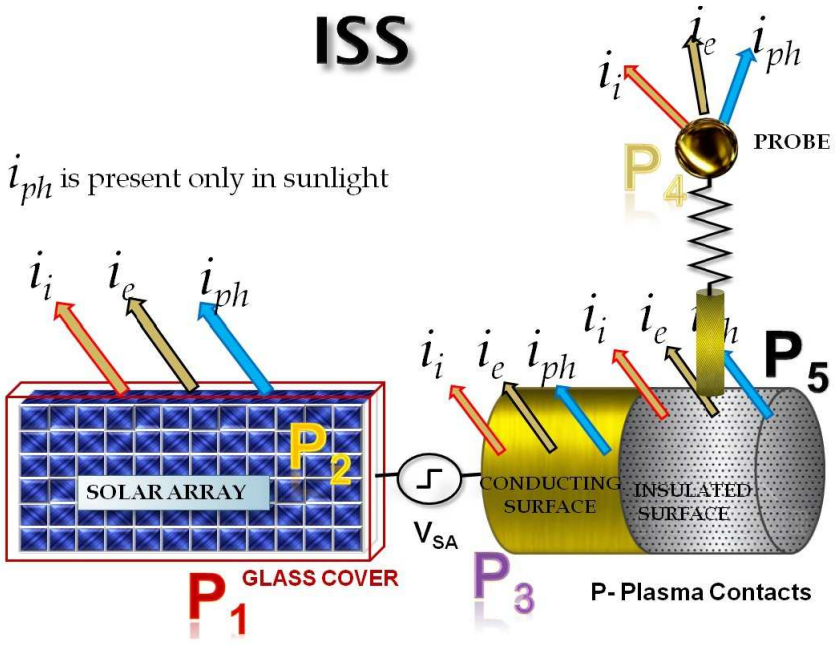

Fig. 2.1: Illustration of collection currents by different surfaces of ISS. i_i, i_e, and i_{ph} denotes the ion current, electron current, and the photoelectron current collected by the different surfaces. i_{ph} is present only when the ISS is in the sunlight. V_{SA} is the solar array voltage source which switches on as soon as ISS enters sunlight. P1, P3, P4, and P5 are points of contact for each surface with plasma where sheath is formed.

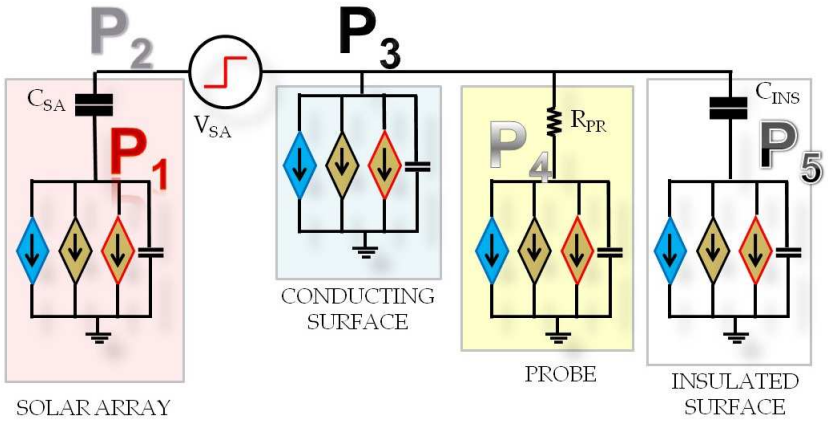

Fig. 2.2: Equivalent electrical circuit where the plasma has been assumed to be at ground potential. The capacitance of the insulated (oxide coated) surface is represented as C_{ISS} and is approximated to 10-11mF (Personal communication with Leonard Kramer, Boeing Corporation). The solar array capacitance C_{SA} is calculated to be 10uF. The red, black, and blue current source represents the ion, electron, and photo current respectively from Fig. 2.1. Resistance R_{PR} separates the probe from ISS body.

it and that the glass cover on top of solar array and the oxide layer on top of oxidized surface will develop some capacitances and store charge. The sheath region also has some capacitance (C_{SHEATH}) and can be modeled as shown in Fig. 2.2. The illustration of Fig. 2.1 can now be reduced to an electrical circuit where collection current sources are combined with sheath capacitance (Barjatya A, 2007) as shown in Fig. 2.2.

Linear Circuit Model

As a first approximation to the nonlinear model for ISS, which is the central subject of this paper, we linearize the nonlinear elements (for now only current sources) as shown in Fig. 2.3. Following this linearization step, we approximate and calculate the sheath capacitances, as given in Table 2.1, and the electrical equivalent system of ISS can be represented as shown in Fig. 2.4(a). The solar array sheath resistance R_{SA}, conducting surface sheath resistance R_{CS}, probe surface sheath resistance $R_{Psheath}$, and insulated surface sheath resistance R_{INS} are shown (the nonlinearity and value of sheath resistances will be discussed later). Because the probe is separated from spacecraft with huge (compared to sheath resistances) impedance, that branch in the circuit does not allow any current through and can be considered practically open. The circuit then reduces from one shown in Fig. 2.4(a) to one in Fig. 2.4(b). The floating potential which is the potential difference across the probe and spacecraft (across nodes marked A', B') is same as across A, B.

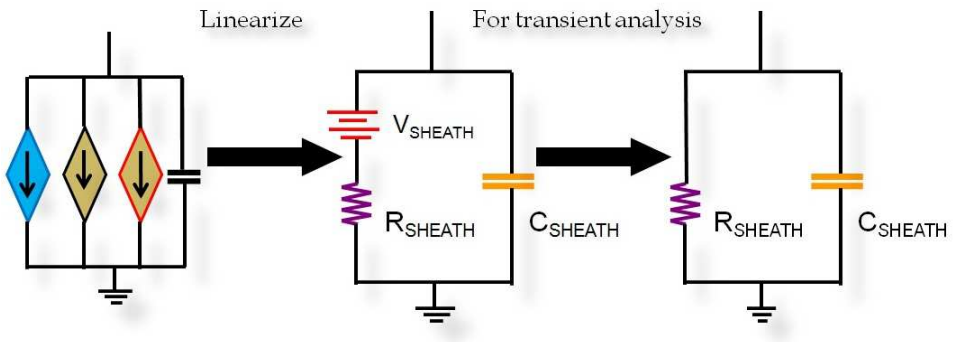

Fig. 2.3: Linearization of the nonlinear model.

Table 2.1: Table showing area of different surfaces and different capacitances. The sheath capacitances are calculated at $n = 1e + 10$ and $T_e = 1000^0 K$.

ISS Components	Area (m^2)	Capacitance (F)	Sheath Capacitance (F)
Solar Arrays	1640	10μ	0.4μ
Conducting Surface	30		$7n$
Insulated Surface	400	10-11m	0.1μ
FPMU FPP Probe	0.01		$2.5pico$

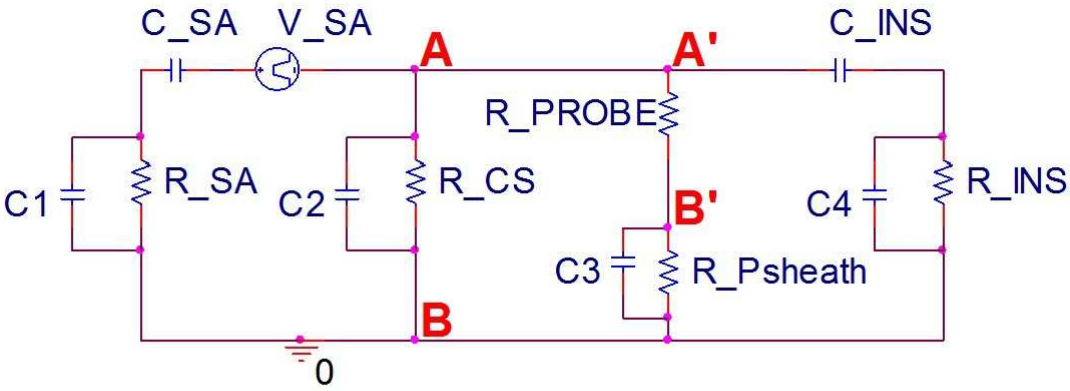

(a)

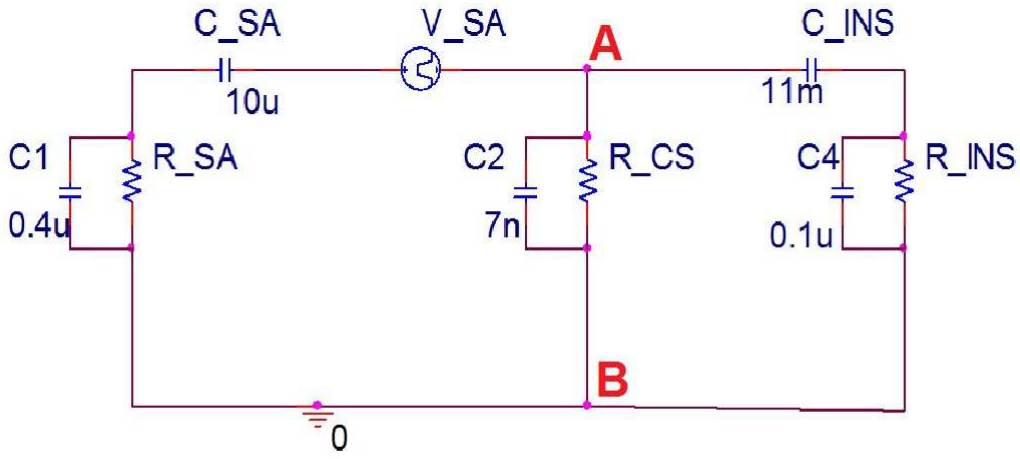

(b)

Fig. 2.4: (a) The top panel shows the linear ISS model. (b) In the bottom panel, the probe section is removed. C1, C2, C3, and C4 are solar array, conducting surface, probe, and insulator sheath capacitances as calculated in Table 2.1.

For simplicity, we assumed all the resistances in this model to be equal (which is definitely not the case as we will discuss later). Different test values have been given to the resistances during simulation run. Because of the large surface area of ISS compared to the solar array glass thickness of millimeter order and oxide thickness of the order of microns, the capacitances are assumed to behave like parallel plate capacitors as shown in Fig. 2.5. The capacitances are calculated as $C = \epsilon_r \epsilon_0 \frac{A}{d}$, where ϵ_r and ϵ_0 are relative and free space permittivity (ϵ_r is used for glass cover on solar array where as for sheath only ϵ_0 is used), A is the area and d is the thickness (Debye length for sheath). All the calculations are given in Table 2.1. The sheath capacitances are calculated at $n = 1e + 10$ and $T_e = 1000^0 K$.

2.2 An Analytic Approach to RCEs

In the previous section we saw how the ISS surface can be divided into conducting (bare metal), anodized (oxidized or insulated), and glass-covered solar arrays. We also learned how these different surfaces draw currents from the surrounding plasma and how and why anodized surface and solar array exhibit capacitances. These collection currents are nonlinear in nature and depend on the surface potential with respect to the surrounding plasma which is again a function of the $V_{ISS} \times B$ field as discussed later in this chapter. In this section, we will try to develop a analytic model for the RCEs using a similar approach of simplified linear electric circuit developed in previous section. This analytical model will give us more insight into the different elements (in the ISS system) which contribute towards the RCE events. Laplace transform and inverse laplace transform will be used to derive the time domain relationship for the charging and discharging voltage. Let us remember the linearization process of the nonlinear collection currents as described in Fig. 2.3. Under transient conditions, we short circuit V_{SHEATH} and the circuit consists of a parallel resistance-capacitance (RC) circuit as shown in the figure. Though the solar array capacitance and anodized surface capacitance are assumed to dominate the RCEs in electric circuit model in previous section, the role and comparison of these capacitances with sheath capacitances of solar array, anodized surface, and solar array will be investigated further in this chapter. The nature and magnitudes of the impedances offered by these different

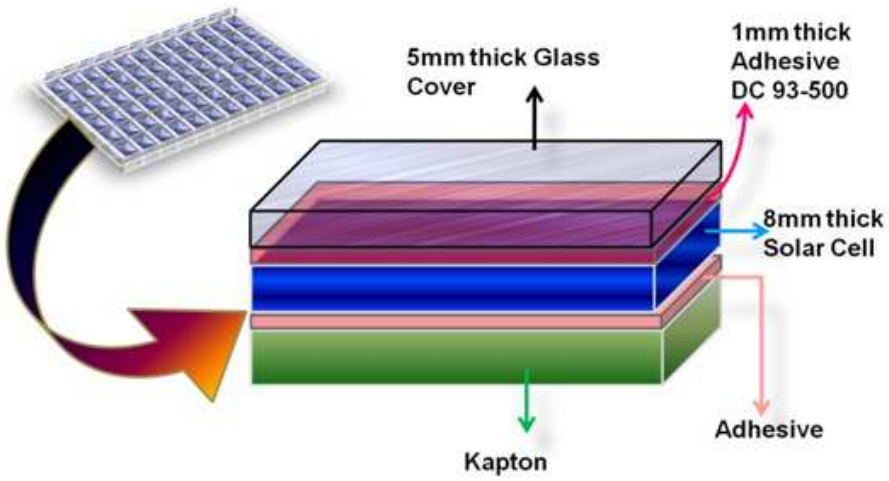

Fig. 2.5: Different layers of solar array

surfaces in the plasma environment will also be discussed.

2.2.1 Linear Model Elements

Capacitances

The ISS equivalent electric circuit contains a capacitance due to the cover glass over solar array, labeled as C_{SA}, a capacitance because of the dielectric materials covering the anodized surfaces, C_{INS}, and the sheath capacitances at each interface between these three surfaces (solar array, bare metal, and anodized) and surrounding plasma. They are labeled as $C1$, $C2$, and $C4$, respectively, in Fig. 2.4(b). The values of C_{SA} and C_{INS} are discussed in previous section and Table 2.1. The sheath capacitances, though has also been assigned some approximate values (see Table 2.1), it is interesting to note that they are functions of surrounding plasma density and temperature. The governing equations for estimating the sheath capacitance is given by

$$C_{SHEATH} = \epsilon_r \epsilon_0 \frac{A}{d}, \tag{2.1}$$

where ϵ_r and ϵ_0 are permittivity of the plasma and free space, A is the surface area and d is the debye's length. The debye's length is given by

$$d = \sqrt{\frac{\epsilon_0 k_b T_e}{ne^2}}, \tag{2.2}$$

where T_e and n are temperature and density of plasma.

To get a better idea, the plot in Fig. 2.6 shows the different capacitances as the plasma density changes at $1000^{\circ}K$ temperature. It is interesting to note that at low density, the sheath capacitances are negligible compared to solar array glass capacitance and oxide layer capacitances. Thus to see the effects of different elements in our mathematical treatment on the system, which is the central purpose of this section we will neglect the sheath capacitances. In other words, we will concentrate on the contribution of C_{SA} and C_{INS} only omitting other capacitances from the system shown in Fig. 2.4(b).

Resistances/Impedances

All the surfaces which are in contact with surrounding space plasma forms sheaths and this region of transition offers some resistances or impedance to the current collection circuit. Impedance offered by a sheath is the inverse of the slope of the I-V curve for the collection current for any surface. Figure 2.7 shows a typical I-V curve for a surface drawing currents from the surrounding plasma (Barjatiya A., 2007). As this I-V curve is nonlinear, it can be easily understood that the impedance varies as we move along the curve from ion-saturation region to the electron retardation region to the electron-saturation region. The value of this impedance given by $\frac{\partial V}{\partial I}$ (where ∂V and ∂I are very small increments in surface potential and collection current on the curve) will be quite high when a surface is operating in any of the saturation regions where as in electron retardation region, it should be comparatively much lower. The variation of impedance at a particular operating point on the I-V curve is also a function of varying density and temperature of the surrounding plasma and the geometry of the colleting surface. For example, for a spherical conductor

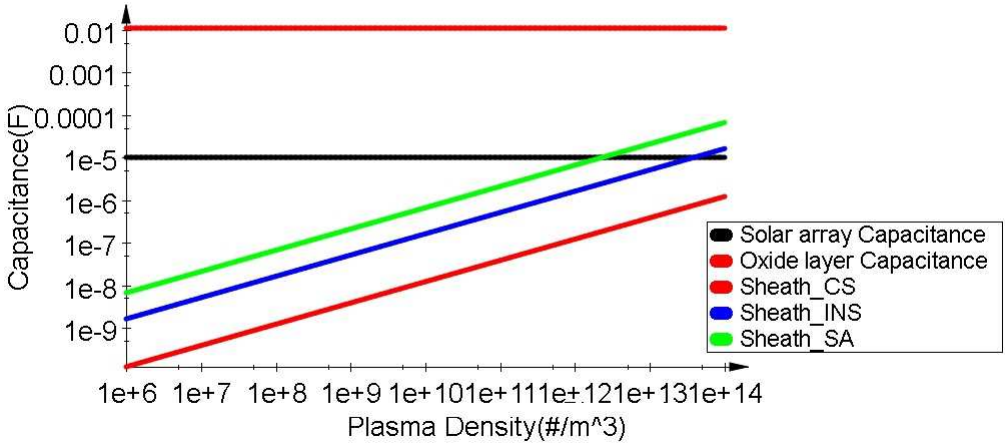

Fig. 2.6: Comparison of solar array, oxide layer, and different sheath capacitances.

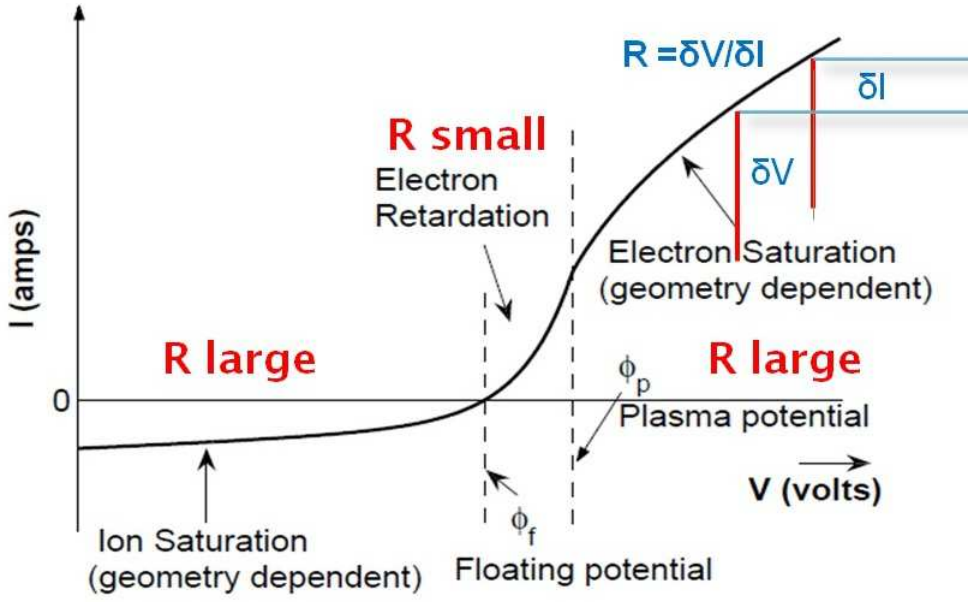

Fig. 2.7: Typical I-V curve of a surface which draws current from the surrounding plasma. The sheath resistance varies depending on the point of operation along the I-V curve.

operating in electron saturation region is given by

$$R = \frac{\partial V}{\partial I} = \frac{k_b T_e}{nAe^2}\sqrt{\frac{2\pi m_e}{k_b T_e}}, \tag{2.3}$$

where T_e, n, A, e, m_e are electron temperature, density, area of the collecting surface, electronic charge, and mass of electron, respectively. The variation of the impedance for a spherical object as a function of density is plotted in Fig. 2.8 at $T_e = 1000°K$. The solar array which predominantly collect electron is assumed to be in electron saturation region where as other surfaces are assumed to be in ion saturation region. From the plot we can estimate that in low-density conditions, the sheath resistances can be of the order of megaohms where as in high density conditions, they become negligibly small. In case of ISS, moving with velocity V_{ISS} in earth's magnetic field B, the $V_{ISS} \times B$ field produced because of its motion in earth's magnetic field imposes a potential gradient over its huge structure which varies depending on its orientation and orbit. Moreover, the solar arrays being biased positively with respect to the ISS body collect electrons from the surrounding space plasma driving them to operate towards in the electron saturation region. This means to complete the current balance in the system, the other parts (conducting and anodized surfaces) must collect ions from the surrounding plasma and will be pushed to operate in the ion-saturation region. Thus we can see that the $V_{ISS} \times B$ and the current balance in the system will make different parts of ISS to operate in different regions on the I-V curve, and thus will exhibit wide range of impedance and floating potential.

2.2.2 Circuit Analysis of Linear Model

Solar Array Driving Signal

The moment ISS comes out in sunlight the solar array voltage source starts kicking the charging system. The signal can be thought as a ramp function as shown in Fig. 2.9 and

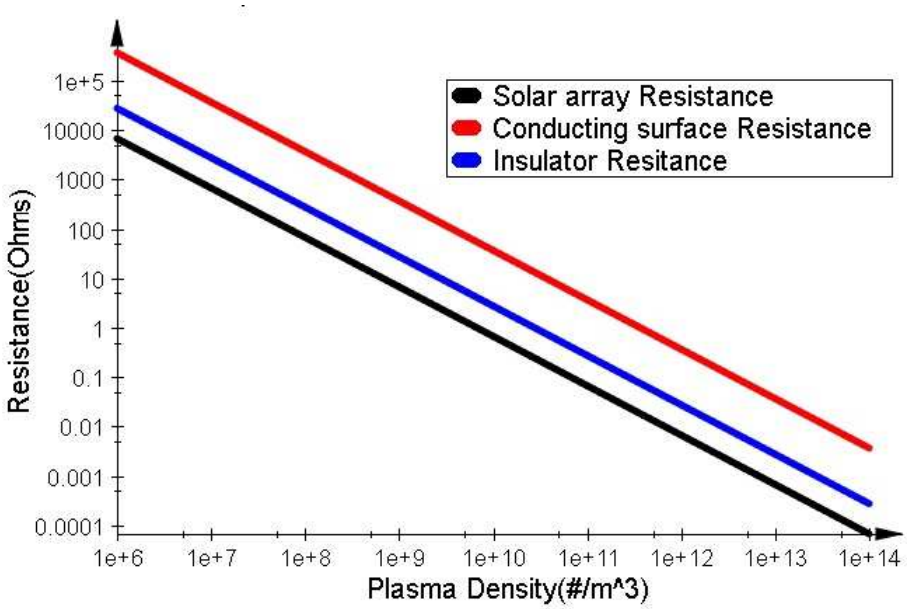

Fig. 2.8: Comparison of solar array, oxide layer, and different plasma sheath resistances. Solar array is assumed to be in electron saturation region where as others in ion saturation region.

given mathematically as

$$V = \begin{cases} 0 & \text{if } t < 0 \\ \frac{K}{t} & \text{if } t < t_1, \\ K & \text{if } t > t_1 \end{cases} \tag{2.4}$$

or $V = Ku(t) - K(t - t_1)u(t - t_1)$, where $u(t)$ denotes a unit step function at $t = 0$.

We, for generality of the problem, will not give any magnitude to the voltage or rising time of the ramp signal.

Few Interesting Circuit Configurations

To get a circuit system which can possibly explain the RCEs on ISS, we start with different configurations with the elements discussed above. The two simplest circuits which can be thought of derivatives from a simple resistance-capacitance (RC) circuit are shown in Fig. 2.10 below.

In the first topology, we consider only the solar array (capacitance C_{SA} and sheath

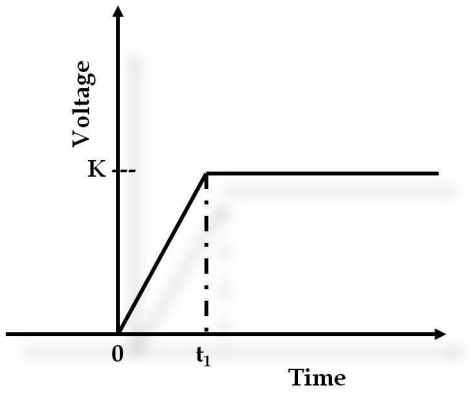

Fig. 2.9: The solar array voltage source function is assumed to be a ramp function.

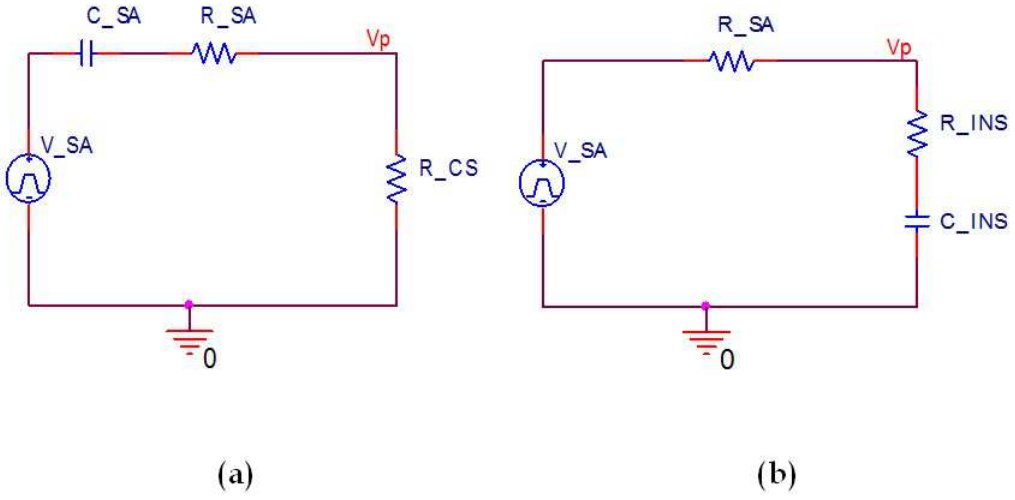

Fig. 2.10: Two simplest circuits derived from a simple RC circuit which describes ISS system.

resistance R_{SA}), and the conducting surface (sheath resistance R_{CS}), eliminate the oxide capacitance C_{INS}, and the oxide sheath resistance R_{INS}. In the second topology we consider only solar array and the anodized surface and eliminate the conducting surface. The idea is to see the effect of both capacitors (solar array and anodized surface) on the full system and which one dominates the occurrence of RCEs. When analyzed in matlab mu-pad program using laplace and inverse laplace transformation for the first schematic (Fig. 2.10(a)), expressions for V_p in time domain is given by

$$V_p = \begin{cases} -C_{SA}R_{CS}\left(\frac{\frac{1}{t}}{e^{C_{SA}(R_{CS}+R_{SA})}} - 1\right) & \text{if } t < t_1 \\ -C_{SA}R_{CS}\left(\frac{\frac{1}{t}}{e^{C_{SA}(R_{CS}+R_{SA})}} - \frac{\frac{1}{t-t_1}}{e^{C_{SA}(R_{CS}+R_{SA})}}\right) & \text{if } t > t_1. \end{cases} \tag{2.5}$$

The output waveform derived from simulation run in SPICE (Simulation Program with Integrated Circuit Emphasis), an industry standard network analysis tool is of the form as shown in Fig. 2.11.

Similarly, for the second schematic (Fig. 2.10(b)), the expression for V_p in time domain is given by

$$V_p = \begin{cases} t - C_{INS}R_{SA} + \frac{C_{INS}R_{SA}}{\frac{t}{e^{C_{INS}(R_{INS}+R_{SA})}}} & \text{if } t < t_1 \\ t_1 + \frac{C_{INS}R_{SA}}{\frac{t}{e^{C_{INS}(R_{INS}+R_{SA})}}} - \frac{C_{INS}R_{SA}}{\frac{t-t_1}{e^{C_{INS}(R_{INS}+R_{SA})}}} & \text{if } t > t_1. \end{cases} \tag{2.6}$$

The output waveform is of the form as shown in Fig. 2.12.

Now for the full system with all the solar arrays, anodized, and conducting surfaces present and sheath capacitances neglected (Fig. 2.13), the expression for $t < t_1$ and $t > t_1$ is huge and is given in the appendix. An output waveform for such a system is plotted using SPICE in Fig. 2.14.

Few interesting things which can be observed from the expressions above are the maximum amplitude of the charging-discharging curve and the importance of rise time of the solar array output ramp function voltage "t_1." It is clear by comparing the output waveforms that it is mainly the solar array capacitance playing a major role in shaping the charging-discharging curve that we see in RCEs. The maximum amplitude of charging

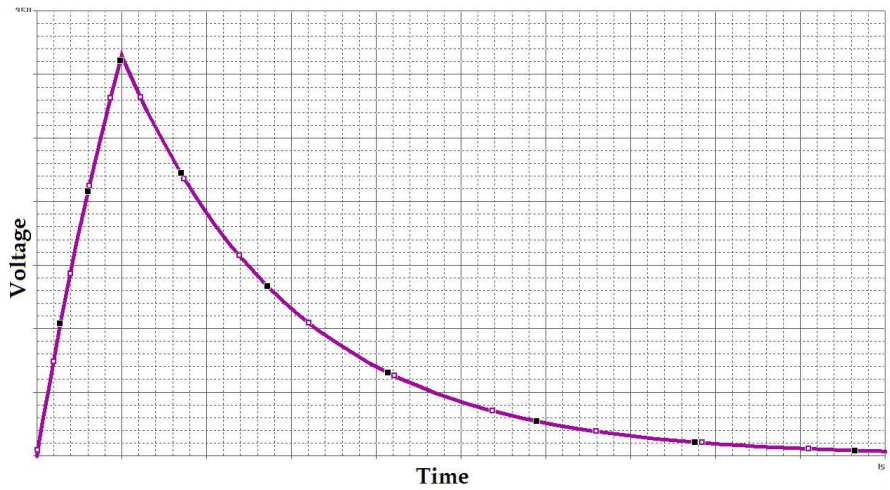

Fig. 2.11: Waveform for a circuit shown in Fig. 2.10(a).

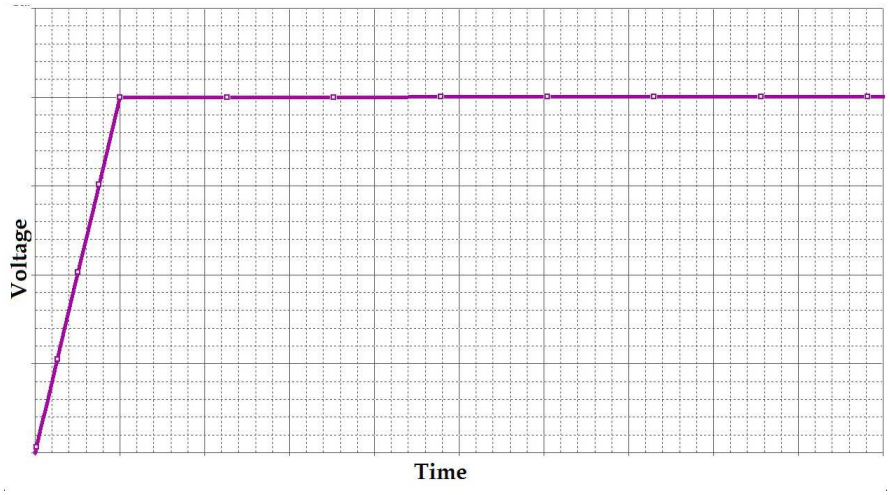

Fig. 2.12: Waveform for a circuit shown in Fig. 2.10(b).

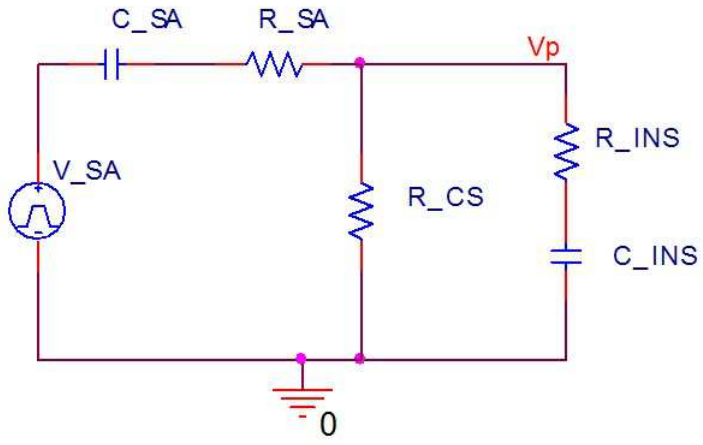

Fig. 2.13: The ISS equivalent circuit.

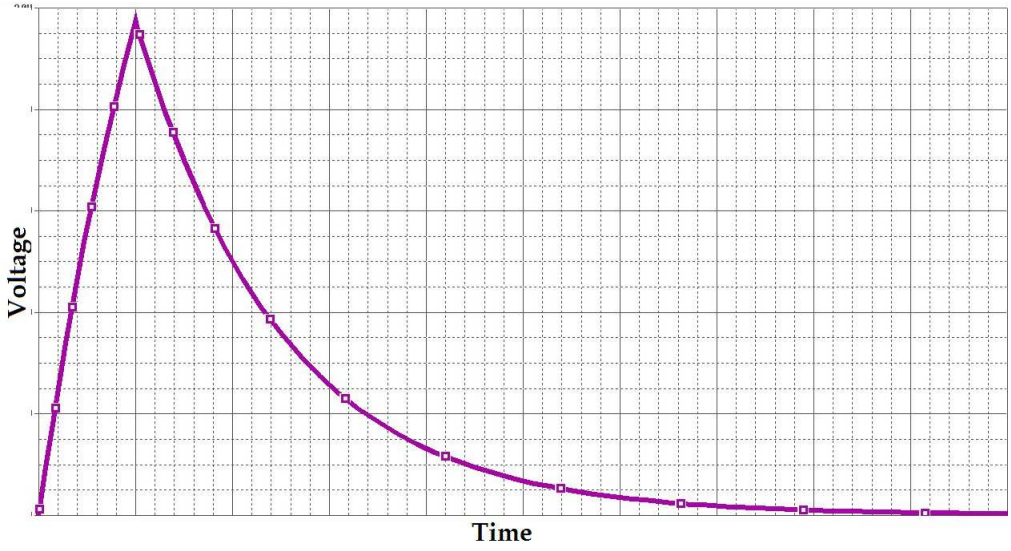

Fig. 2.14: Waveform for a circuit shown in Fig. 2.13.

pulse is derived by putting $t = t_1$ in the expression for $t_1 > t$ in the last case (Fig. 2.13). The comparatively bigger anodized surface capacitance does not seem to play any important for shaping these charging-discharging events except for the "knee" feature in the discharge phase which will be discussed in the next chapter. Also clearly t_1, i.e., the rising time of the ramp signal from solar array, plays a very important role in deciding the rise time to the peak charging level in the charging-discharging observed.

Chapter 3

Simulations and Results

The model, as shown in Fig. 2.4(b), is simulated in SPICE (Simulation Program with Integrated Circuit Emphasis), an industry standard network analysis tool. The circuit is driven with a ramp signal V_{SA} with 1sec rising time and amplitude 80V. This voltage pulse emulates the surge in solar array voltage source as soon as ISS exits earth's shadow and enters sunlight. We approximated all the resistances in the circuit to be equal and calculated capacitances as described in previous section. Using the values, shown in Fig. 2.4(b), and setting all the sheath resistances equal to a test value of $10M\Omega$, we get the RCE fluctuation of floating potential as shown in Fig. 3.1.

The plot shows that the ISS floating potential (Y-axis) drops by -38V from background value as soon as ISS comes into sunlight. It takes about 35secs for this charging level to subside back to normal level. Figure 3.2(a) and (b) compare data with model. The data plot is reproduced from literature [1]. It is interesting to note that the discharge curve clearly shows two storage elements ("knee" feature in Fig. 3.2) which can be because of presence of two capacitors C_{INS} and C_{SA}. In Fig. 3.3(a), (b), and (c) are shown the results of similar simulations but with resistance values changed to 50meg, 1meg, and 1K Ohms, respectively. It is evident from the simulations, the amplitude of the RCEs and the discharge time varies with resistances. We believe that this is exactly what is happening on ISS: the combined capacitive and resistive surface is responsible for this sudden charging discharging effect on eclipse exit. The low-density condition pushes this further by changing the capacitance and resistance values.

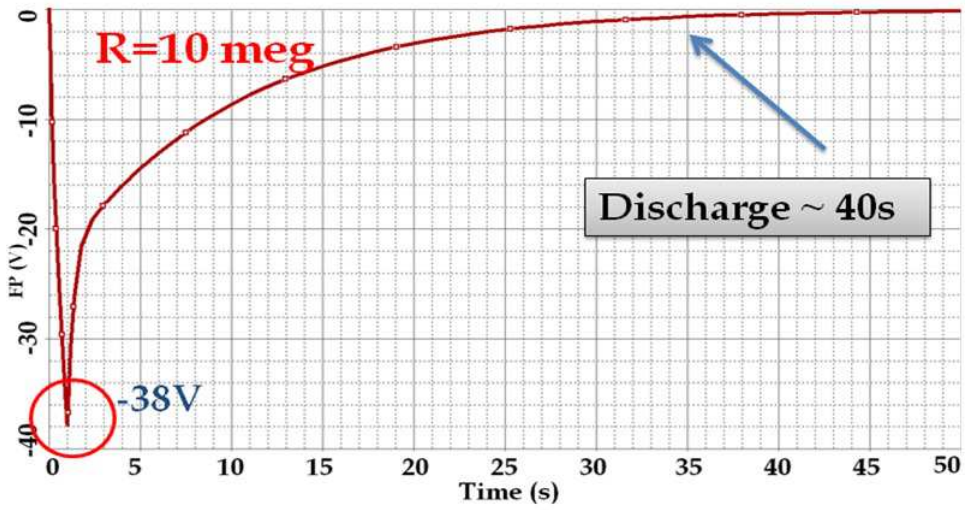

Fig. 3.1: RCE simulation with all resistances equal to 10meg. The floating potential (FP) surges to -38V from its normal value and discharges over 40secs.

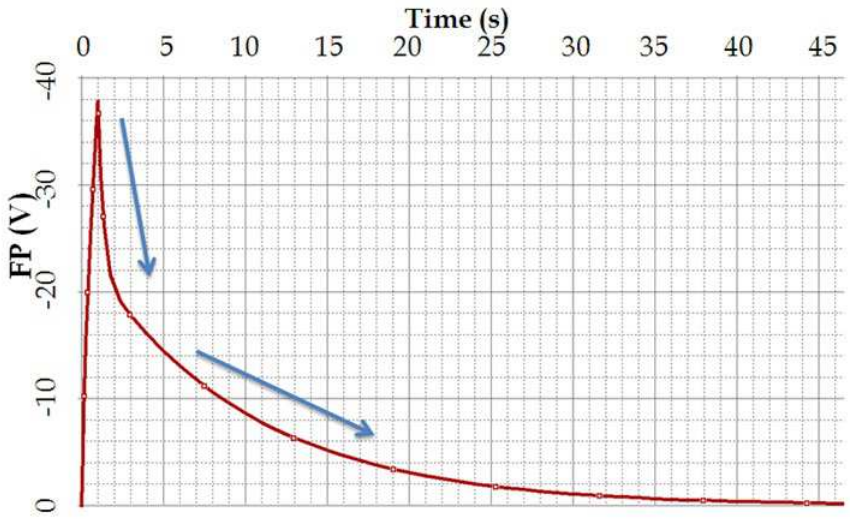

(a)

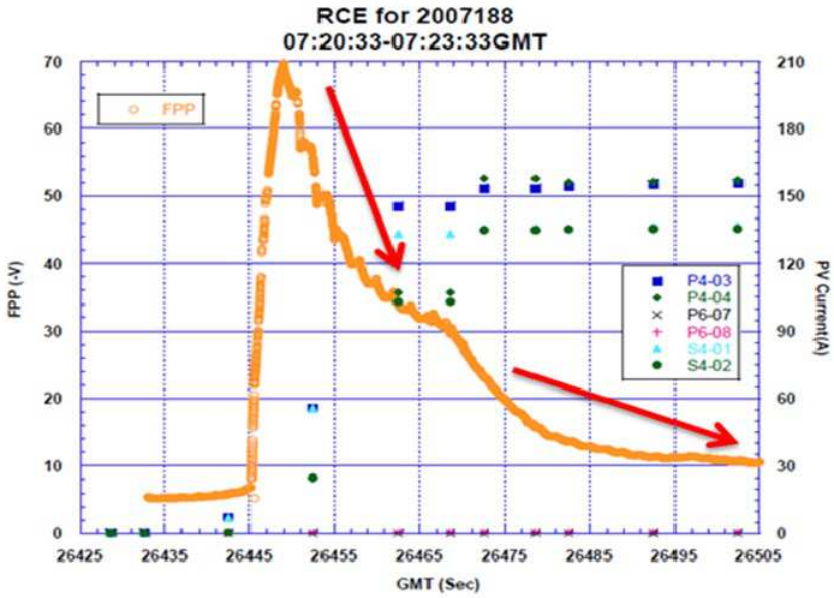

(b)

Fig. 3.2: (a) Top and (b) bottom panel: Model vs data. The presence of two different time constants is marked by arrows.

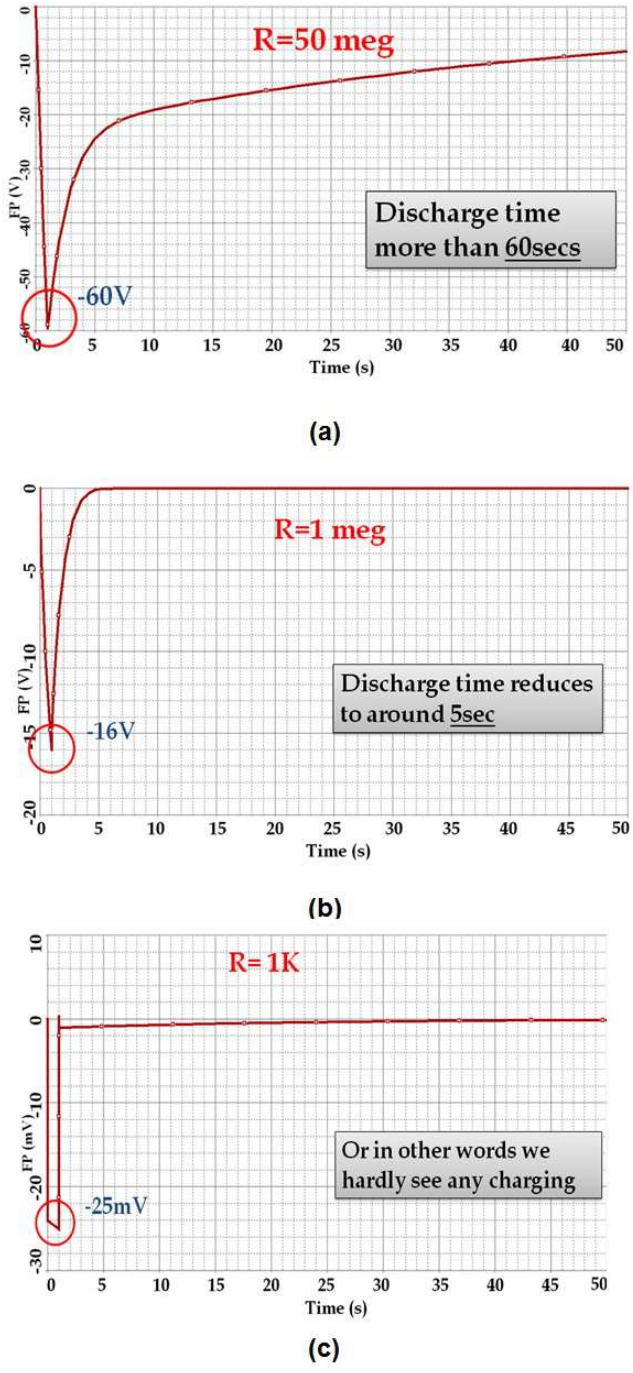

Fig. 3.3: (a) Top, (b) middle, and (c) bottom panel: Simulation results for different resistance values.

Chapter 4

Conclusions and Discussions

This report builds a simplistic model for the RCEs observed on ISS and other big spacecrafts. When the target is to have a deeper understanding of the observed phenomenon, the simple linear model fails to address the cause of occurrence of such events in depleted regions in certain longitude sectors. We strongly believe that this is because of the nonlinearity of the sheath resistances and capacitances which are functions of surrounding density, temperature, surface areas, ion species, etc., and are not reflected in the simple linear model. It is tempting to suspect that at the morning terminator sunlight produces more photoelectrons in the low-density region than the ambient plasma ions or electrons. This sudden surge in electrons pushes the station into more negative potential. But our experiment with the nonlinear model of which the linear model reported here is a derivative have shown that photoelectrons are not the cause of RCEs. It is the electrical properties (capacitance and resistance) of the ISS structure that are responsible for RCEs. We tried to analyze the contribution from all the sub-systems, namely, the solar array, conducting surface, insulated surface, and the probe and concluded that it is the solar array capacitance and the sheath resistances of different surfaces which are responsible for RCEs. An easy suspect for such storage of charge could have been the huge insulated surface capacitance. But our investigations does show that the insulated surface capacitance does not contribute to such RCEs except for contributing towards changing the discharge curve mentioned as "knee" feature which was observed when insulated section was included (Fig. 3.2). It has been observed through simulation results that if the solar array capacitances can be reduced, both the amplitude and discharge time of the RCE events can be reduced, thus reducing the threat on the spacecraft. This means for the solar array, if we remember the equation for solar array capacitance: $C = \epsilon_r \epsilon_0 \frac{A}{d}$, increasing the thickness of the glass since reducing

the area is ruled out because of need for more and more power for ISS. But the problem of increasing the glass thickness means increase in total weight of the spacecraft. The RCEs data observed onboard are functions of many plasma parameters and the geometry and orientation of ISS in the earth's magnetic field. We strongly believe that with the knowledge gained from this simple linear model, the next step will be to develop the full nonlinear model, shown in Fig. 2.2, which will include most of the corrections that are not addressed in this linear model.

References

[1] P. Craven, K. Wright Jr, J. Minow, V. Coffey, T. Schneider, J. Vaughn, D. Ferguson, and L. Parker, "Survey of international space station charging events," in *47th AIAA Aerospace Sciences Meeting Including The New Horizons Forum and Aerospace Exposition*, Orlando, FL, Jan. 2009.

[2] J. I. Minow, K. H. Wright Jr, M. Chandler, V. N. Coffey, P. D. Craven, T. A. Schneider, L. N. Parker, D. C. Ferguson, S. L. Koontz, and J. W. Alred, "Summary of 2006 to 2010 fpmu measurements of international space station frame potential variations," in *11th Spacecraft Charging Technology Conference*, Albuquerque, NM, Sept. 2010.

[3] H. Kamwahi and M. Patterson, "On the operational status of the international space station plasma contactor hollow cathodes," in *41st AIAA/ASME/SAE/ASEE Joint Propulsion Conference & Exhibit*, pp. 1–15, 2005.

[4] C. M. Swenson, D. Thompson, and C. Fish, "The floating potential measurement unit," in *41st AIAA Aerospace Sciences Meeting and Exhibit*, Reno, NV, Jan. 2003.

[5] C. S. C. Fish and D. Thompson, "Calibrating the floating potential measurement unit," in *8th Spacecraft Charging Technology Conference*, Huntsville, AL, Jan. 2003.

[6] C. M. Swenson, D. Thompson, and C. Fish, "The ISS floating potential measurement unit," in *9th Spacecraft Charging Technology Conference*, Tsukuba, Japan, 2005.

[7] K. H. Wright, C. M. Swenson, D. C. Thompson, A. Barjatya, S. L. Koontz, T. A. Schneider, J. Vaughn, J. I. Minow, P. D. Craven, V. N. Coffey, L. N. Parker, and T. H. Bui, "Charging of the international space station as observed by the floating potential measurement unit: Initial results," *IEEE Transactions on Plasma Science*, vol. 36, no. 5, pp. 2280–2293, 2008.

[8] D. C. Ferguson, G. B. Hillard, T. L. Morton, and R. Personen, "ISS FPP ionospheric electron density and temperature measurements: Results, comparison with the iri-90 model, and implications for iss charging," in *41st AIAA Aerospace Sciences Meeting and Exhibit*, Reno, NV, Jan. 2003.

[9] G. Matticari, M. Materassi, G. E. Noci, A. Severi, and J. Sabbagh, "PLEGPAY: Plasma contactor experiment on the international space station," in *International Electric Propulsion Conference*, Pasadena, CA, 2001.

[10] M. J. Mandell and V. Davis, "Electron collection by international space station solar arrays," in *8th Spacecraft Charging Technology Conference*, Huntsville, AL, 2003.

[11] H. Barsamian, R. Mikatarian, J. Alred, J. Minow, and S. Koontz, "ISS plasma interaction: Measurements and modeling," in *8th Spacecraft Charging Technology Conference*, Huntsville, AL, 2003.

[12] H. Jeong, *Kinetic Simulations of Spacecraft Charging and Plasma Interactions in the Solar Wind*. Ph.D. dissertation, Virginia Polytechnic Institute and State University, 2008.

[13] A. Barjatya, *Langmuir probe measurements in the ionosphere*. Ph.D. dissertation, Utah State University, 2008.

[14] L. H. Brace, "Langmuir probe measurements in the ionosphere," *Washington DC: American Geophysical Union*, 1998.

[15] D. C. Ferguson, "Fpp results final report," *Plasma Science, IEEE Transactions on Plasma Science*, vol. 37, no. 2, pp. 369–374, 2009.

[16] D. C. Ferguson, P. Craven, J. I. Minow, and K. H. W. Jr, "A theory for rapid charging events on the international space station," in *1st AIAA Atmospheric and Space Environments Conference*, San Antonio, TX, 2009.

Appendix

Few important resistance-capacitance circuits

This appendix contains the necessary circuit analysis for few resistance-capacitance circuit discussed in Chapter 3 in this report.

A) To start with we consider a simple network with a single resistance and a single capacitance as shown in Fig. A.1. Voltage across R in s domain is given by $V(s)$. Then using inverse laplace transformation, we determine the time domain expression for voltage across R. This is defined by $V(t)$ for the time $t < t_1$ and ($V_1(t)$ for $t > t_1$. The mupad program in matlab is given in Fig. A.2.

B) Now we introduce another resistance in the above circuit as shown in Fig. A.2 below. In this topology, C_{SA} and R_{SA} denotes the solar array capacitance and resistance respectively where as R_{CS} denotes the resistance offered by the conducting surface. We find the voltage across R_{CS}, which is the voltage measured by FPP (see Section 2.1). Using a similar treatment like above, we determine the time domain voltage. Here, V_p in Fig. A.3 denotes the time domain voltage measured by the probe (the mupad program is given in Fig. A.4.

C) The third topology we consider is shown below in Fig. A.5. Here we remove the solar array capacitor and replace the conducting surface with anodized surface capacitance C_{INS} and anodized surface resistance R_{INS} (the mupad program is given in Fig. A.6).

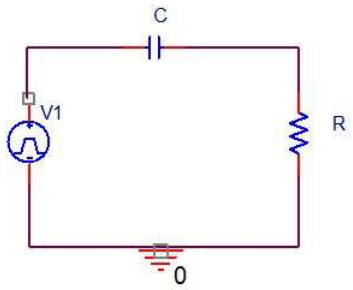

Fig. A.1: A simple RC circuit.

```
V(s):= (R)/(R+1/(s*C))*1/s^2
```

$$\frac{R}{s^2\left(R+\frac{1}{Cs}\right)}$$

```
Vss := partfrac(V(s),s,Full)
```

$$\frac{CR}{s}-\frac{C^2R^2}{CRs+1}$$

```
V(t):= transform::invlaplace(Vss, s, t)
```

$$CR-\frac{CR}{e^{\frac{t}{CR}}}$$

This is the expression for t<t_1

```
simplify(V(t))
```

$$-CR\left(\frac{1}{e^{\frac{t}{CR}}}-1\right)$$

```
V_1(t) := V(t) - subs(V(t), t=(t-t_1))
```

$$\frac{CR}{e^{\frac{t-t_1}{CR}}}-\frac{CR}{e^{\frac{t}{CR}}}$$

This is the expression for t > t_1

```
simplify(V_1(t))
```

$$-CR\left(\frac{1}{e^{\frac{t}{CR}}}-\frac{1}{e^{\frac{t-t_1}{CR}}}\right)$$

Fig. A.2: Mupad program for circuit in Fig. A.1.

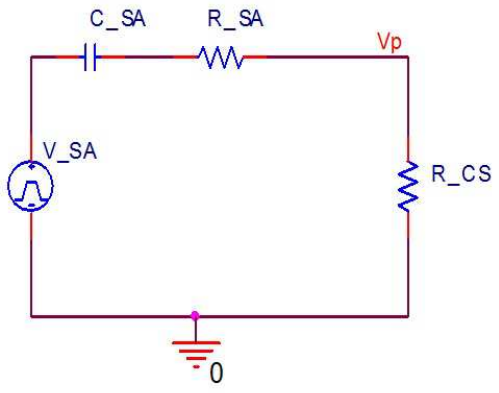

Fig. A.3: Circuit with one more resistance added to Fig. A.1.

```
V(s):= (R_C_S)/(R_S_A +R_C_S+1/(s*C_S_A))*1/s^2
```

$$\frac{R_{CS}}{s^2\left(R_{CS}+R_{SA}+\frac{1}{C_{SA}s}\right)}$$

```
Vss:= partfrac(V(s),s,Full)
```

$$\frac{C_{SA}R_{CS}}{s}-\frac{{C_{SA}}^2R_{CS}(R_{CS}+R_{SA})}{s(C_{SA}R_{CS}+C_{SA}R_{SA})+1}$$

```
V(t):= transform::invlaplace(Vss, s, t)
```

$$C_{SA}R_{CS}-\frac{{C_{SA}}^2R_{CS}(R_{CS}+R_{SA})}{e^{\frac{t}{C_{SA}R_{CS}+C_{SA}R_{SA}}}(C_{SA}R_{CS}+C_{SA}R_{SA})}$$

This is the expression for t<t_1

```
simplify(V(t))
```

$$-C_{SA}R_{CS}\left(\frac{1}{e^{\frac{t}{C_{SA}(R_{CS}+R_{SA})}}}-1\right)$$

```
V_1(t):= V(t) - subs(V(t), t=(t-t_1))
```

$$\frac{{C_{SA}}^2R_{CS}(R_{CS}+R_{SA})}{e^{\frac{t-t_1}{C_{SA}R_{CS}+C_{SA}R_{SA}}}(C_{SA}R_{CS}+C_{SA}R_{SA})}-\frac{{C_{SA}}^2R_{CS}(R_{CS}+R_{SA})}{e^{\frac{t}{C_{SA}R_{CS}+C_{SA}R_{SA}}}(C_{SA}R_{CS}+C_{SA}R_{SA})}$$

This is the expression for t > t_1

```
simplify(V_1(t))
```

$$-C_{SA}R_{CS}\left(\frac{1}{e^{\frac{t}{C_{SA}(R_{CS}+R_{SA})}}}-\frac{1}{e^{\frac{t-t_1}{C_{SA}(R_{CS}+R_{SA})}}}\right)$$

Fig. A.4: Mupad program for circuit in Fig. A.3.

D) Now lets integrate the full system by including solar array, conducting surface, and anodized surface. A equivalent circuit is shown in the following Fig. A.7.

The expression for $V(t)$ and $V_1(t)$ can also be found similarly as were done in a), b), and c). It is not included here for the expressions are too big to be accommodated here.

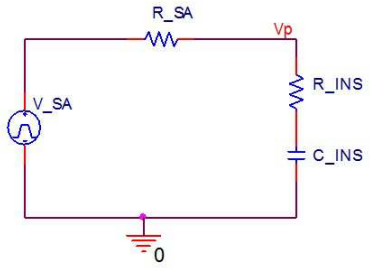

Fig. A.5: Another variation to Fig. A.3 where the capacitor is placed across the output.

```
V(s):= (R_I_N_S + 1/(s*C_I_N_S))/(R_S_A +R_I_N_S+1/(s*C_I_N_S))*1/s^2
```

$$\frac{R_{INS}+\frac{1}{C_{INS}\,s}}{s^2\left(R_{INS}+R_{SA}+\frac{1}{C_{INS}\,s}\right)}$$

```
Vss := partfrac(V(s),s)
```

$$\frac{1}{s^2}-\frac{C_{INS}\,R_{SA}}{s}+\frac{C_{INS}^{\,2}\,R_{SA}\,(R_{INS}+R_{SA})}{s\,(C_{INS}\,R_{INS}+C_{INS}\,R_{SA})+1}$$

```
V(t):= transform::invlaplace(Vss, s, t)
```

$$t-C_{INS}\,R_{SA}+\frac{C_{INS}^{\,2}\,R_{SA}\,(R_{INS}+R_{SA})}{e^{\frac{t}{C_{INS}\,R_{INS}+C_{INS}\,R_{SA}}}\,(C_{INS}\,R_{INS}+C_{INS}\,R_{SA})}$$

```
simplify(V(t))
```

$$t-C_{INS}\,R_{SA}+\frac{C_{INS}\,R_{SA}}{e^{\frac{t}{C_{INS}\,(R_{INS}+R_{SA})}}}$$

```
V_1(t):= V(t) - subs(V(t), t=(t-t_1))
```

$$t_1-\frac{C_{INS}^{\,2}\,R_{SA}\,(R_{INS}+R_{SA})}{e^{\frac{t-t_1}{C_{INS}\,R_{INS}+C_{INS}\,R_{SA}}}\,(C_{INS}\,R_{INS}+C_{INS}\,R_{SA})}+\frac{C_{INS}^{\,2}\,R_{SA}\,(R_{INS}+R_{SA})}{e^{\frac{t}{C_{INS}\,R_{INS}+C_{INS}\,R_{SA}}}\,(C_{INS}\,R_{INS}+C_{INS}\,R_{SA})}$$

```
simplify(V_1(t))
```

$$t_1+\frac{C_{INS}\,R_{SA}}{e^{\frac{t}{C_{INS}\,(R_{INS}+R_{SA})}}}-\frac{C_{INS}\,R_{SA}}{e^{\frac{t-t_1}{C_{INS}\,(R_{INS}+R_{SA})}}}$$

Fig. A.6: Mupad program for circuit in Fig. A.5.

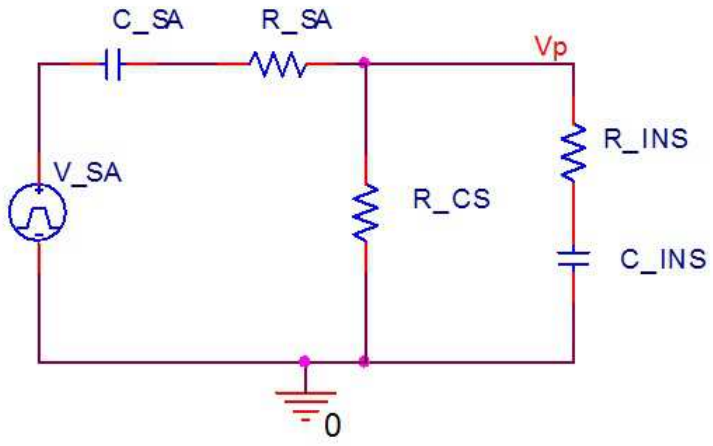

Fig. A.7: ISS equivalent circuit.

V(s):= (v(s))/(R_S_A + 1/(s*C_S_A)+ v(s))*1/s^2

$$\frac{R_{CS}\left(R_{INS}+\frac{1}{C_{INS}s}\right)}{s^2\left(R_{CS}+R_{INS}+\frac{1}{C_{INS}s}\right)\left(R_{SA}+\frac{1}{C_{SA}s}+\frac{R_{CS}\left(R_{INS}+\frac{1}{C_{INS}s}\right)}{R_{CS}+R_{INS}+\frac{1}{C_{INS}s}}\right)}$$

Fig. A.8: Expression for V(s) for circuit in Fig. A.7.